Journal of Applied Polymer Science

REVIEW

Nanostructured piezoelectric polymers

Valentina Cauda,[1] Giancarlo Canavese,[1] Stefano Stassi[2]

[1]Center for Space Human Robotics IIT@PoliTo, Corso Trento 21, Torino 10129, Italy

[2]Department of Applied Science and Technology, Politecnico di Torino, Corso Duca degli Abruzzi 24, Torino 10129, Italy

Correspondence to: V. Cauda (E-mail: valentina.cauda@iit.it)

ABSTRACT: Among the wide variety of piezoelectric materials available, polymers offer an interesting solution because of their high mechanical flexibility, easy processing, and conformable features; they maintain good ferroelectric and piezoelectric properties. The most prominent examples of these are poly(vinylidene fluoride) (PVDF) and its copolymer, poly(vinylidene difluoride–trifluoroethylene) [P(VDF–TrFE)]. An attractive prospective consists of the preparation of nanostructured polymers. It has been shown that the dimensional confinement of such macromolecules down to the nanoscale can improve their piezoelectric properties because the tailoring of the chemical structure is performed at the molecular level. In this review, we show how nanostructured polymers can be obtained and discuss reports on the ferroelectric and piezoelectric properties of nanostructured PVDF and P(VDF–TrFE) materials. In particular, we show how dimensional confinement leads to piezoelectric nanostructures with relevant performances, with a focus on the macromolecular structural arrangement that enhances their behavior. Experimental results and applications are also reported to compare the performances of different nanostructuration processes and the polymer efficiencies as piezoelectric materials. © 2014 Wiley Periodicals, Inc. J. Appl. Polym. Sci. **2015**, *132*, 41667.

KEYWORDS: crystallization; nanostructured polymers; phase behavior; properties and characterization; sensors and actuators

Received 19 September 2014; accepted 27 October 2014

DOI: 10.1002/app.41667

INTRODUCTION

Polymeric materials can be easily tailored at the nanoscale to achieve low-temperature and relatively low-cost processing structures with a high flexibility, light weight, and easy deformation properties. For all these advantages, they have recently raised great interest among the scientific community, offering new and promising solutions for the fabrication of novel polymer-based devices in the fields of electronics,[1] microelectronics,[2] sensing,[3] photonics,[4] adhesion,[5] and biotechnology.[6]

The development and integration of such nanostructured polymers have progressed rapidly in the last decade, but only recently has the size-dependent structure of such macromolecules been explored. Studies on dimensional confinement have revealed that geometrically confined polymers can greatly deviate in their physical behavior, such as crystallization[7] or chain dynamics,[8] from their bulk counterpart. In particular, arrays of polymeric nanostructures showing ferroelectric and piezoelectric behavior, as in the case of both poly(vinylidene fluoride) (PVDF) and its copolymers with trifluoroethylene {poly(vinylidene fluoride–trifluoroethylene) [P(VDF–TrFE)]}, have raised tremendous interest for the fabrication of miniaturized and novel organic electronic devices, such as high-density nonvolatile memories,[7] nanogenerators,[2] field-effect transistors,[9] tactile and IR imaging sensors,[2] acoustic sound transducers,[10] capacitors,[11,12] and solar cells.[13,14]

The PVDF polymer can crystallize in five different phases, called the α, β, γ, δ, and ε phases,[15,16] among which the α phase is nonpolar and the β phase is the most polar. The copolymer P(VDF–TrFE) crystallizes predominantly in the β phase, readily showing an intrinsic polarization. However, because of the semicrystalline nature of these polymers, PVDF–TrFE can also present a paraelectric phase, even after polymer annealing.[17]

The advantage of using piezoelectric polymers in applications such as nonvolatile memories, sensors, and energy nanogenerators, instead of conventional piezoelectric ceramics (e.g., lead zirconium titanate, also called PZT, or $BaTiO_3$) includes their excellent solution and low-temperature processing, high flexibility and conformability, high electric breakdown field, light weight, and nontoxicity. However, piezoelectric polymers show reduced piezoelectric properties, that is, piezoelectric constant (d_{33}) values, with respect to their ceramic counterparts.

Recently, it was shown that geometrical confinement, which leads to a high-aspect-ratio PVDF and P(VDF–TrFE) nanostructures with at least one feature size below 100 nm, has a profound influence on the final piezoelectric performances of these macromolecules. In particular, preferential crystallization in the

Valentina Cauda works as senior post doc at the Istituto Italiano di Tecnologia in Turin, Italy. She received her Ph.D. in material science and technology in 2008 from Politecnico di Torino, Italy, and graduated with a degree in chemical engineering in 2004. From 2008 to 2010, she worked as a post doc at the Faculty of Chemistry, University of Munich, Germany. She is involved in the chemical synthesis and characterization of polymeric and oxide-based nanostructures for piezoelectric and sensing applications.

Giancarlo Canavese is a researcher at the Istituto Italiano di Tecnologia in Turin, Italy. He received his M.E. degree in mechanical engineering in 2004 and his Ph.D. degree in biomedical engineering in 2008 from Politecnico di Torino. In 2013–2014, he worked for 6 months as a visiting researcher at the Houston Methodist Research Institute, Texas. His areas of interest include piezoresistive composite materials, Micro Electro-Mechanical Systems (MEMS) technologies, and the distribution of tactile sensors for robotic applications.

Stefano Stassi works as a post doc researcher at the Department of Applied Science and Technology, Politecnico di Torino in Torino, Italy. He received his M.S. degree in nanotechnology engineering and his Ph.D.in physics from Politecnico di Torino and Istituto Italiano di Tecnologia, Torino, Italy, in 2009 and 2013, respectively. His current research interests include Micro Electro-Mechanical Systems (MEMS) resonating sensor fabrication, and integration for biomedical analysis, preparation, and characterization of piezoresistive and piezoelectric materials and metal nanoparticle synthesis.

polar β phase was shown not only in P(VDF–TrFE) nanostructures[17] but also in PVDF nanowire arrays, and it led to remarkable levels of polarization[18,19] without further processing the polymer with mechanical stretching or electrical poling, in contrast to the polymer's conventional performance in bulk or thin films. Indeed, the possibility of preventing the poling step represents a great advantage, not only in terms of time and equipment but also because these polymers can be prepared as a ready-to-use and device-integrated functional materials without any further processing. Actually, the poling process can be critical in terms of applied voltages and temperature conditions for electronic circuits if they are integrated with the piezoelectric polymers. Moreover, the enhancement of the piezoelectric properties due to nanostructuration results in an increased d_{33}, lower coercive field, and uniform switching behavior.[1,18]

In this review, we aim to give an overview of the most recent advances in piezoelectric polymeric nanostructures, from the synthetic approach to various application fields. Among the different fabrication methods, the template-assisted infiltration, nanoimprinting or nanoembossing with a mold, and electrospinning techniques are reviewed. Importantly, we study the geometrical confinement down to the nanometer level to determine its effect on the chain preferential orientation and crystallization of both the PVDF and P(VDF–TrFE) polymers. Characterization methods, such as piezoresponse force microscopy (PFM), and the interesting ferroelectric and piezoelectric properties of nanostructured polymeric arrays are also presented here. Finally, an overview of the applications that have been explored in the literature is also given.

SYNTHESIS TECHNIQUES

Nanostructures of piezoelectric polymers are typically synthesized by three main techniques: template-assisted infiltration with the use of a porous matrix or membrane, electrospinning, and nanoimprinting with a mold; these all lead to excellent results in terms of both nanostructuration and size-dependent piezoelectric properties. All of these methods start from the PVDF of the P(VDF–TrFE) polymers in pellet form and either use them at the melting point (ca. 250°C) or dissolved in an organic solvent, typically a mixture of dimethylformamide and acetone for PVDF and methyl ethyl ketone for P(VDF–TrFE). In the following sections, each method is discussed in detail.

Template-Assisted Approach

The template-assisted approach consists of the infiltration of a porous host matrix by the polymer melt or solution. The polymer spreads onto the pore walls of the templating matrix to form a thin film. Then, it preferentially starts nucleation and growth on this surface; this results in nanotubes for short infiltration times or low supplied materials. In contrast, the formation of nanowires results from the complete filling of the

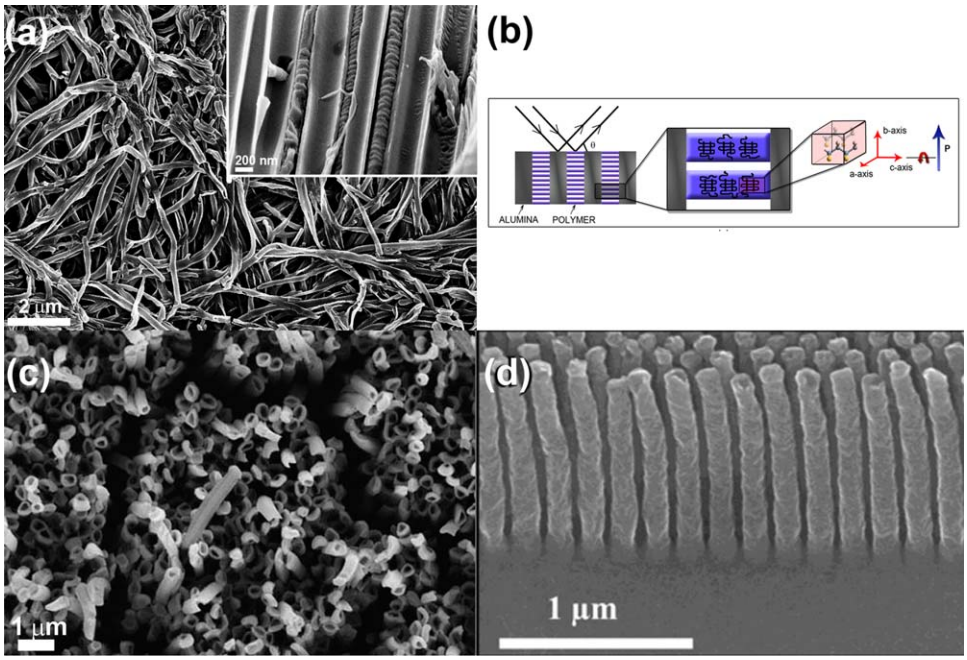

Figure 1. (a) P(VDF–TrFE) nanowires after the removal of the templating alumina matrix (inset: needlelike polymeric crystals stacked perpendicularly to the long axis of the P(VDF–TrFE) nanowires). (b) Scheme of the polymeric crystalline structure arrangement and polarization direction. θ is the incidence angle of the X-ray diffraction beam used for the structural characterization of the polymeric nanowires. Reprinted with permission from ref. 18. Copyright 2013 American Chemical Society. (c) Nanotubes of P(VDF–TrFE). Reprinted with permission from ref. 80. Copyright 2006 Elsevier. (d) Self-standing P(VDF–TrFE) nanorods from immersion crystallization method. Reprinted from ref. 4. Copyright 2012 Wiley-VCH. P = polarization. [Color figure can be viewed in the online issue, which is available at wileyonlinelibrary.com.]

template pore and stops when either the solvent evaporates or the polymer melt quenches.[3]

To obtain an array of vertically oriented nanowires or nanotubes, porous matrixes with nanosized pores, all aligned parallel to the matrix thickness and possibly with uniform size, are used. The most common host for such purposes is anodic porous alumina (APA) membranes, obtained from the anodization of thin aluminum films or sheets.[20,21] The pores are highly uniform in size and spacing (mainly arranged with a hexagonal symmetry) and open at both ends.

Examples of APA template wetting by the polymeric solution have been reported in several works.[3,17,22] Depending on the process used for the APA impregnation, that is, vacuum impregnation, spin coating, or solution casting, all followed by proper thermal treatments, vertically oriented nanotubes or nanowires showing uniform diameter distribution and very high aspect ratios have easily been obtained. Typical arrays of both nanowires and nanotubes are shown in Figure 1.

Some disadvantages of the template-assisted approach include a difficulty in large-area fabrication, scalability, and sometimes, pore size uniformity. Problems of entanglement and the leaning of the nanostructures when the template is removed are inevitable in the APA template-assisted method because of the extremely high aspect ratio. Recently, to solve this problem, an SiO_2 template having nanopores of about 120 nm in diameter and 1.2 μm in length and fabricated by a photolithography technique and etching was used.[4] An interesting immersion crystallization method was efficiently applied so that the template removal and polymer crystallization were simultaneously accomplished by immersion of the sample in a hot etching solution at 100°C for 1 h. In this way, self-standing and aligned P(VDF–TrFE) nanowires were obtained, as shown in Figure 1(d).

Among the less common porous hosts, mesoporous silica, that is, micelle-templated porous SiO_2 with pore sizes ranging from 2 to 15 nm[23,24] [as reported, e.g., in Figure 2(a)], and mesoporous organosilica (OS)[25,26] have been efficiently used to confine polymers such as PVDF and P(VDF–TrFE)[1,19] and obtain enhanced piezoelectric performances.

An example of these templates was the ultrathin polymeric nanowires embedded in the oriented mesoporous silica; they showed an unprecedented high aspect ratio and were just 5 or 10 nm in diameter, depending on the surfactant-templated mesoporous silica used, and up to 60 μm long [Figure 2(b)].[19] They were obtained from the deposition of an organic solution with a low polymer concentration *in vacuo* to help with the infiltration by the tiny mesopores. In contrast, spin coating applied to such templates cannot properly infiltrate the long mesoporous channels, whereas it works properly with the horizontal mesoporous OS trenches reported by Kang *et al.*,[1] where the channels were flat on the substrate [Figure 2(c)]. In this case, the nanopatterned trenches were completely filled by the spun P(VDF–TrFE) polymer.

The crystalline structure of the template-nanostructured polymers and, thus, the macromolecular orientation can be evidenced from characterization measurements such as wide-angle X-ray scattering (WAXS) and IR spectroscopy. As an example, the inset of Figure 2(b) shows the WAXS pattern of bulk PVDF

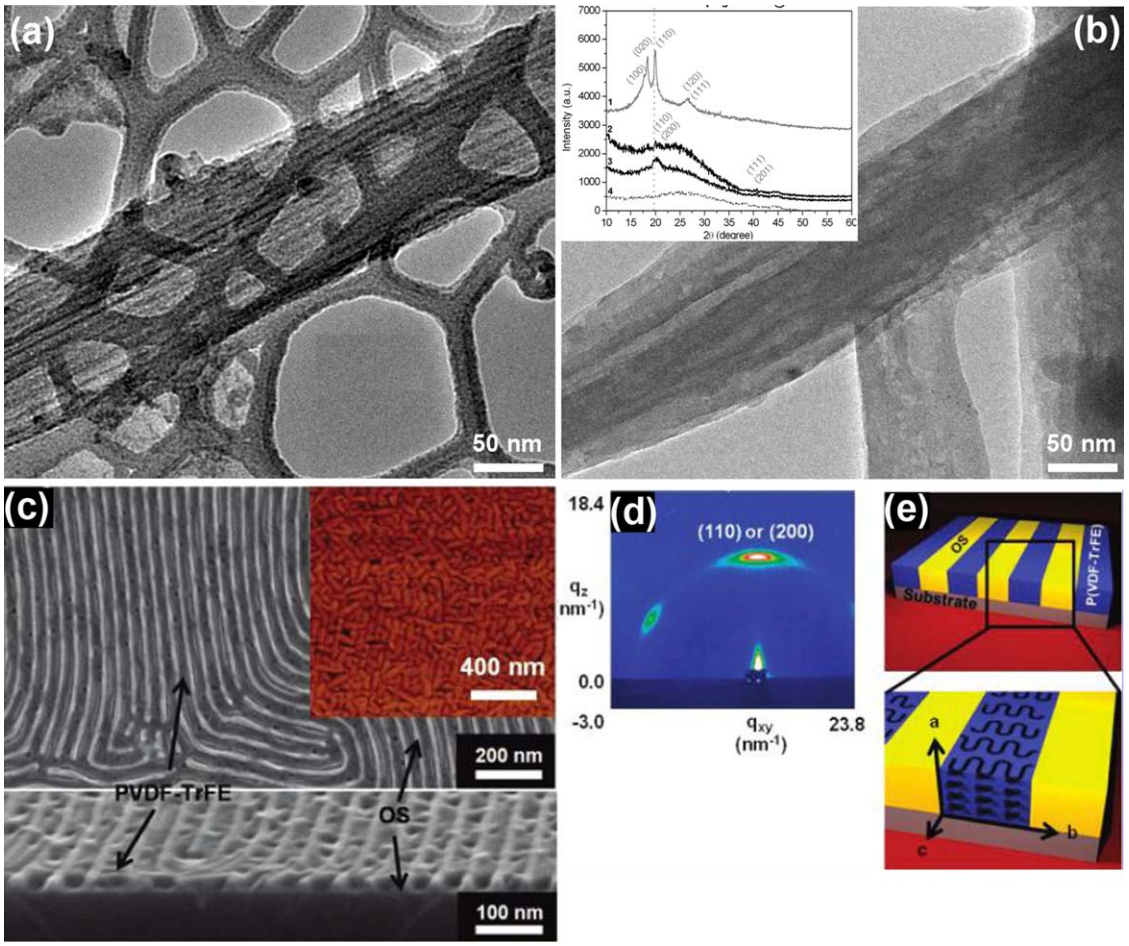

Figure 2. (a) Transmission electron microscopy of a mesoporous silica filament 5 nm in pore diameter and (b) bundle of PVDF ultrathin nanowires after template dissolution. Inset of the (b) X-ray diffraction pattern of bulk PVDF (curve 1)-confined PVDF nanowires in 5-nm pores (curve 2) and 10-nm pores (curve 3), empty mesoporous silica host template (curve 4) (Reprinted with permission from ref. 19. Copyright 2012 American Chemical Society). (c) Scanning electron micrograph of OS lamellae in top and cross-sectional views filled with P(VDF–TrFE) [inset: AFM topographic image of a P(VDF–TrFE) film formed on nanopatterned OS]. (d) 2D GIWAXS pattern of the confined P(VDF–TrFE) in nanopatterned OS. q_{xy} and q_z are the scattering vectors in the directions x,y along the sample surface plane and z normal to the surface plane. (e) Schematic illustration of the preferential orientation of the confined P(VDF–TrFE) crystals in nanopatterned OS. Reprinted with permission from ref. 1. Copyright 2013 American Chemical Society. [Color figure can be viewed in the online issue, which is available at wileyonlinelibrary.com.]

polymer in the form of a thin film with typical diffraction peaks belonging to the α nonpolar phase (curve 1). Interestingly, both spectra (curves 2 and 3) belonging to the ultrathin nanowires, templated into both 5- and 10-nm mesopore hosts, showed only the peaks assigned to the β ferroelectric phase. It could be assumed that the extreme PVDF confinement into the mesopores induced a clear preferential orientation of the crystalline units according to the β polar phase. Similarly, the two-dimensional (2D) grazing incidence wide-angle X-ray scattering (GIWAXS) pattern of nanostructured P(VDF–TrFE) in OS trenches, as shown in Figure 2(d), clearly showed an intense reflection on the meridian, corresponding to the preferred (110) or (200) β crystals, and another reflection tilted at 60° off from the meridian. This pattern indicated that the P(VDF–TrFE) crystals had a preferential orientation when confined in OS nanopatterns, and in particular, they were aligned along the trenches and perpendicular to the polymer chains lying on the surface, as shown in Figure 2(e).

The macromolecular arrangement and its crystallization in confined geometries have been studied deeply previously and have shown good agreement between experimental studies[18,19,27] and molecular simulations.[28] In particular, when the size of the nanostructured host met or was even below the size of the polymer crystallites, the nanoconfinement produced a preferential orientation in the semicrystalline polymer, whatever the type of polymer. It was reported that when slippery, the repulsive hard walls of the host were involved, and at high crystallization temperatures, the crystal nucleation and growth of the polymer was favored in the direction parallel to the flat surface of the walls.[28] This was the case in hydrophilic alumina or silica walls, which showed a repulsive effect with respect to the highly hydrophobic PVDF and P(VDF–TrFE) polymers. Indeed, the crystallographic *b* axis showed the fastest growth direction in the PVDF polymer, and experimental evidence also showed the clear presence of needlelike polymeric crystals stacked

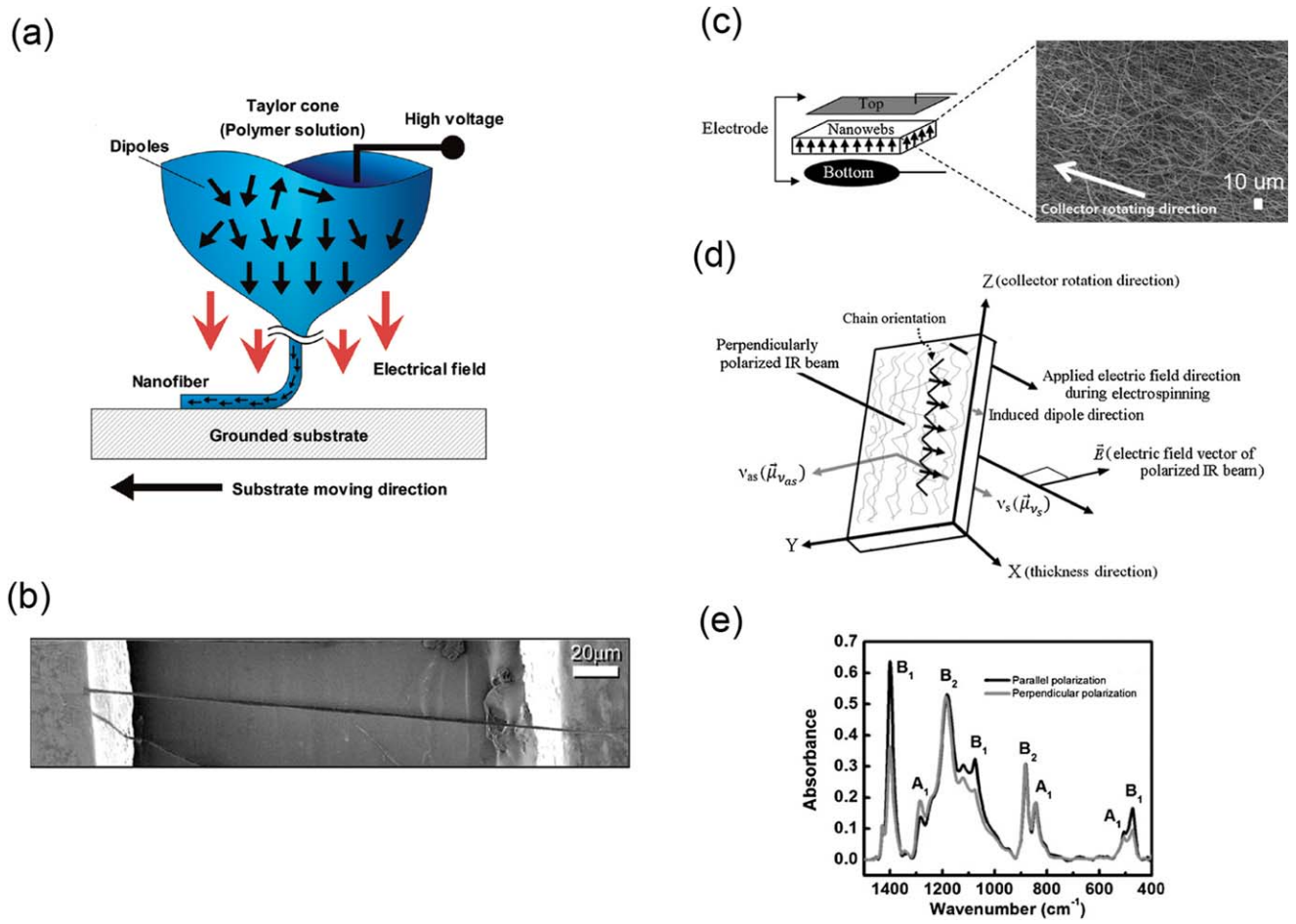

Figure 3. (a) Near-field electrospinning applied on the PVDF polymer with the combination of direct-write, mechanical stretching, and *in situ* electrical poling. (b) Scanning electron microscopy (SEM) image of a single PVDF nanofiber on a plastic substrate. Reprinted from ref. 2. Copyright 2011 Wiley-VCH. (c) Scheme of a nanofiber web (left top) from an electrospinning technique on a rotating substrate with an SEM view of the P(VDF–TrFE) nanofiber web (right top). (d) Scheme of the chain orientation of the P(VDF–TrFE) nanofiber web depicted in part (c), showing the direction of the perpendicularly polarized IR beam, the electric field vector *E* of the incident IR beam, and the vibrational transition modes of the electroactive dipoles. μ_{as} (asymmetric stretching) and μ_s (symmettric stretching) of $-CH_2$ groups, where ν_{as} and ν_s are the vibrational moment of asymmetric and symmetric stretching, respectively. *X* is the sample thickness direction, *Y* is the sample plane direction and *Z* the collector rotation direction. (e) IR spectra of an as-electrospun P(VDF–TrFE) nanofiber web measured with parallel and perpendicular polarized IR beams. Reprinted with permission from ref. 5. Copyright 2010 American Chemical Society. [Color figure can be viewed in the online issue, which is available at wileyonlinelibrary.com.]

perpendicularly to the long axis of the P(VDF–TrFE) nanowires confined in 200-nm pores of the anodic alumina membrane [see the inset of Figure 1(a)].[18] A needlelike crystals is composed of multiple stacks of crystalline lamellae along its axis direction, having the *a* and *c* axes in plane with the crystalline lamellae and the *b* axis perpendicular to them, as shown in Figure 1(b). When these results were combined with the X-ray diffraction patterns, it came out that the *b* axis was thus parallel to the long axis of the template channel.[18,19,27] The *a* and *c* axes were perpendicular to the alumina channel axis; thus, the formation of the nuclei flat on the surface was facilitated [Figure 1(b)].

In addition, the dipole moment of the polymer turned on the *c* axis, and thus, the polarization was maximized along the nanowire axis upon the application of an electric field in the direction perpendicular to the template surface. Therefore, the preferred orientation of the chain *c* axis upon nanoconfinement into the porous template led to favorable ferroelectric and piezoelectric properties along the nanowire axis, as described later. This resulted in a unnecessary poling of the polymeric nanowires, usually carried out in the case of bulk or thin films to obtain a good piezoelectric response.[29–31]

A conflicting issue concerning the orientation of the polar *b* axis in the copolymer crystalline structure was recently proven for P(VDF–TrFE) thin films[32] and confined nanostructures into porous alumina[33] by electron diffraction techniques. In both cases, the crystallographic *a* axis was aligned along the surface of either the substrate or the templating channel because of the fastest growth direction of the P(VDF–TrFE) crystals. A possible explanation of these apparent contrasting results resided in the details of the thermal treatments applied during the crystallization of the P(VDF–TrFE) copolymer, which strongly influenced the orientation of the crystalline lamellae, as reported for ultrathin films.[34]

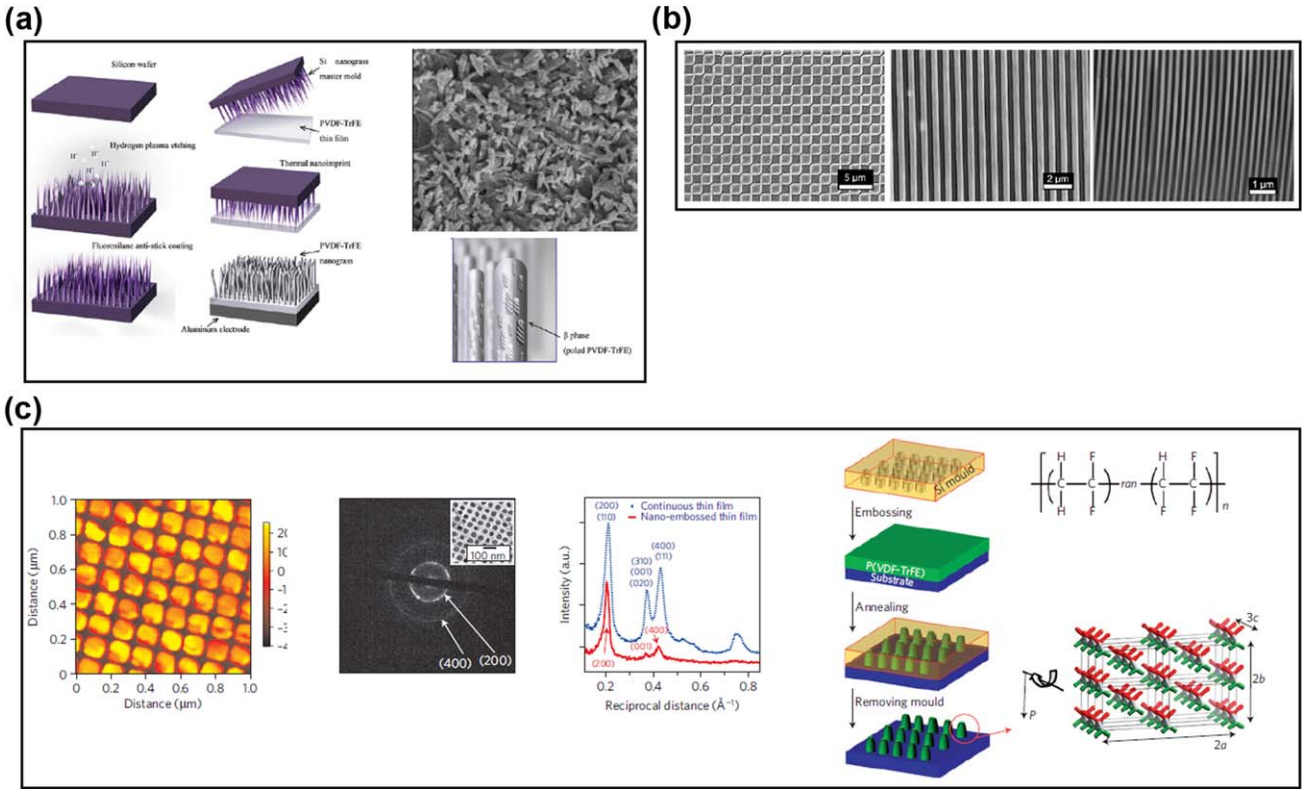

Figure 4. (a) Left panels: Scheme of the fabrication process for obtaining P(VDF−TrFE) nanograss starting from the fabrication of a silicon nanograss mold (in violet), then the imprinting of the P(VDF−TrFE) polymer film into nanograss, and finally its poling. Right panels: SEM image of the imprinted nanograss and scheme of the crystalline orientation of the β crystals after the poling step. Reprinted with permission from ref. 6. Copyright 2012 American Chemical Society. (b) SEM images of the nanoimprinted P(VDf–TrFE) with a (left) 2D square pattern, one-dimensional line pattern with feature sizes of (center) 417 nm and (right) 139 nm. Reprinted with permission from ref. 8. Copyright 2010 American Chemical Society. (c) (From left to right) AFM topography image of the nanoembossed cells showing a high density of nanostructures, electron diffraction patterns, and corresponding transmission electron microscopy image in the inset of the nanostructures. IR spectroscopy of the nanostructures (solid red line) and of a continuous film (dotted blue line) as reference. Nanoembossing fabrication process of high-density arrays of crystalline P(VDF–TrFE) nanostructures and chemical repeat units of the P(VDF–TrFE) copolymer and final orientation of the crystal unit cell of the P(VDF–TrFE) copolymer after embossing with a vertical polar *b* axis and in-plane *a* and *c* axes. Reprinted with permission from ref. 7. Copyright 2008 Macmillan. [Color figure can be viewed in the online issue, which is available at wileyonlinelibrary.com.]

Electrospinning

Piezoelectric polymeric nanofibers can also be obtained by electrospinning. This simple and scalable process is a bottom-up approach, where an intense electric field (>107 V/m) is applied to a cone containing the polymeric solution. The polymer is then forced to be extruded through a nozzle and deposited on a grounded substrate, which is under rotational or translational movements [Figure 3(a)]. The strong mechanical stretching and electrical poling during the electrospinning process align the dipoles of the nanofiber crystal. In the case of the PVDF polymer, the nonpolar α phase, having a random orientation of dipoles, is transformed into the polar β phase; this leads to a polar and oriented electrospun nanofiber. Further processes such as direct-contact poling or corona poling inducing spontaneous dipolar orientation, can be eliminated.

As-spun PVDF nanofibers were obtained with diameters ranging from 500 nm to 6.5 μm with variable lengths,[5] depending on the distance between the electrospinning electrodes [Figure 3(b)].

Mandal *et al.*[2] studied electrospun P(VDF–TrFE) nanofibers by IR spectroscopy to elucidate the spontaneous dipole orientation during the electrospinning process. These authors obtained nanofibers with an average diameter ranging from 60 to 120 nm and found that the preferential fiber orientation was along the substrate rotation direction, as depicted in Figure 3(c). Indeed, the IR spectra of the electrospun nanofiber webs [Figure 3(e)], measured by both perpendicular and parallel polarized beams, showed the A1 (symmetric stretching vibrations of CF_2) and B2 (antisymmetric stretching and rocking vibrations of CF_2) absorption bands in the perpendicular polarized spectrum, whereas the B1 absorption band (wagging vibrations of CH_2) was predominant in the parallel polarized spectrum. Therefore, the P(VDF–TrFE) fiber resulted, with the CF_2 dipoles oriented perpendicular to the polymer chain, as shown in Figure 3(d).

Nanoimprinting or Nanoembossing Lithography

Regular arrays of piezoelectric nanostructures in the form of nanopillars and nanowires can be obtained by nanoimprinting techniques. Nanoimprinting lithography is used to replicate the inverse patterns of master structures, mainly made of silicon. In both the nanoimprinting and nanoembossing techniques,

generally, a thin film of the polymer is obtained by the spin coating of the polymeric solution with an organic solvent. Then, the nanostructured mold is hot-pressed at a molding temperature above the polymer's glass-transition temperature with a hydraulic hot-press machine consisting of heating and pressing components. Particular attention should be paid to ferroelectric polymers, where the hot-embossing temperature has to be above the Curie temperature but below the melting point. The mold and the polymeric film deposited on a wafer are heated and then pressed together at about 1 MPa to hot-press emboss the polymeric nanostructures and thus extrude the softened polymer material to fill the nanocavities in the mold. After molding, the sample should cool gradually to room temperature, and generally, the nanostructures are able to self-detach from the master mold.

With this technique, Hong *et al.*[6] prepared ferroelectric P(VDF−TrFE) copolymer nanograss structures with a diameter of 19 nm and a length of 169 nm with a silicon master mold [Figure 4(a), left panels]. Despite the ease of reproducibility of the method and the one-step fabrication process, these modest aspect ratio (8.9) of P(VDF−TrFE) nanopillars partially collapsed after nanoimprinting [Figure 4(a), right panels]. In addition, the poling of the ferroelectric copolymers had to be applied to obtain a sufficient piezoelectric response; thus, a preparation step was added.

Regular arrays of polycrystalline ferroelectric P(VDF–TrFE) patterns over a large area were obtained by Liu *et al.*[8] Either 2D square patterns or one-dimensional line patterns, with the finest feature size of 139 nm, were fabricated by the nanoimprinting technique in only 3 min at a temperature of about 135°C [Figure 4(b)]. Remarkably, the authors did not apply any postimprinting annealing process, such as electric poling, to achieve good piezoelectricity of the nanostructured P(VDF–TrFE) linear pattern. However, no discussion about the polymer chain orientation was reported, even though the authors assumed that the pressure applied during the imprinting process would help the crystallization of the polymer, in particular at the valleys and bases of the nanostructures. Other authors[35] found that the nanoembossing process could significantly improve the crystallinity and orientation of the P(VDF–TrFE) films.

With a similar approach, Hu *et al.*[7] reported a rapid nanoembossing process that led to a highly nanostructured pattern of 100 nm high nanocells [Figure 4(c)], starting from a 50 nm thick P(VDF–TrFE) thin film. In contrast to the previous studies, these authors deeply studied the macromolecular chain orientation upon nanodimensional confinement. The obtained electron diffraction patterns of the nanostructures were compatible with a vertical orientation of the polar *b* axis and an in-plane orientation of the *a* and *c* axes. In addition, the IR spectrum [Figure 4(c), in red] of the nanoembossed cells showed the extinction of the A1 band at 1288 cm^{-1} (symmetric stretching vibrations of CF_2, having a transition dipole moment parallel to the polar *b* axis). This indicated that the *b* axis was strongly tilted away from the substrate in the nanoimprinted structures. In contrast, both the B1 band at 1400 cm^{-1} (wagging vibrations of CH_2, transition dipole moment μ_c parallel to the *c*-axis of the polymer chain) and the 1187-cm^{-1} B2 band (antisymmetric stretching and rocking vibrations of CF_2, having the transition dipole moment ν_a parallel to the *a*-axis of the polymer) increased in the nanoimprinted cells with respect to the reference film (spectrum in blue); this indicated an in-plane orientation of the *a* and *c* axes.

As mentioned previously, because the dipole moment rotated on the *c* axis upon the application of a vertical electric field, the polarization vector was perpendicular to the substrate; this effectively eased the switching of the polarization. Each nanocell was, thus, composed of a crystalline monodomain, and all nanocells were equivalent. No poling was, therefore, necessary in this case to obtain a good piezoresponse because of the preferential polymer orientation. However, the authors observed that the piezoresponse amplitude was further enhanced by poling with a downward electric field. This indicated that the total dipole moment of the P(VDF–TrFE) crystals was not completely vertically aligned in the nanostructures before poling, probably because of the contributions of more disordered regions, such as the interfaces, where the *b* axis may not have been vertically oriented after imprinting

In general, two key issues have been identified as responsible for obtaining a strong improvement in the ferroelectric properties.[7] The first is the reduction to zero of the thickness of the residual layer at the bottom of the nanostructures that could still contain many crystals of different orientations. Second, the size of nanoconfinement should be of the same order of magnitude of the polymeric crystal size, which will thus prevent the heterogeneous nucleation of the polymer.[36]

Other Methods

A method alternative to the previously reported methods for obtaining arrays of PVDF nanowires was recently reported[37] with a novel thermal melt-drawing method. This approach consists of an iterative size-reduction process, which results in the multiple axial elongation and radial reduction of a starting macroscopic polymeric rod. The obtained millimetric fibers from the first thermal size-reduction step are then cut and arranged in hexagonal lattices inside a protective jacket of a thermoplastic polymer, vacuum-consolidated, and redrawn. This second step reduces the wire size to a few micrometers. The drawing step is repeated a third time, and thus, an array of coaxial nanowires and nanotubes of flexible polymer fibers is obtained with diameters below 15 nm. This method, in particular, allowed the authors to obtain indefinitely long PVDF nanowires with uniform size for hundreds of meters that were radially homogeneous in the cross section. However, no further insights into the crystalline structure or about the eventual polarization orientation were given.

FERROELECTRIC AND PIEZOELECTRIC PROPERTIES

PVDF and its copolymer P(VDF–TrFE) show an intrinsic permanent dipole moment and, thus, remarkable ferroelectric properties induced by the spatial arrangement of the chain segments in the crystalline phase.[15,38] The most pronounced ferroelectric behavior of PVDF is shown when it crystallizes in the polar β phase.[39–41] In this configuration, the unit cell presents

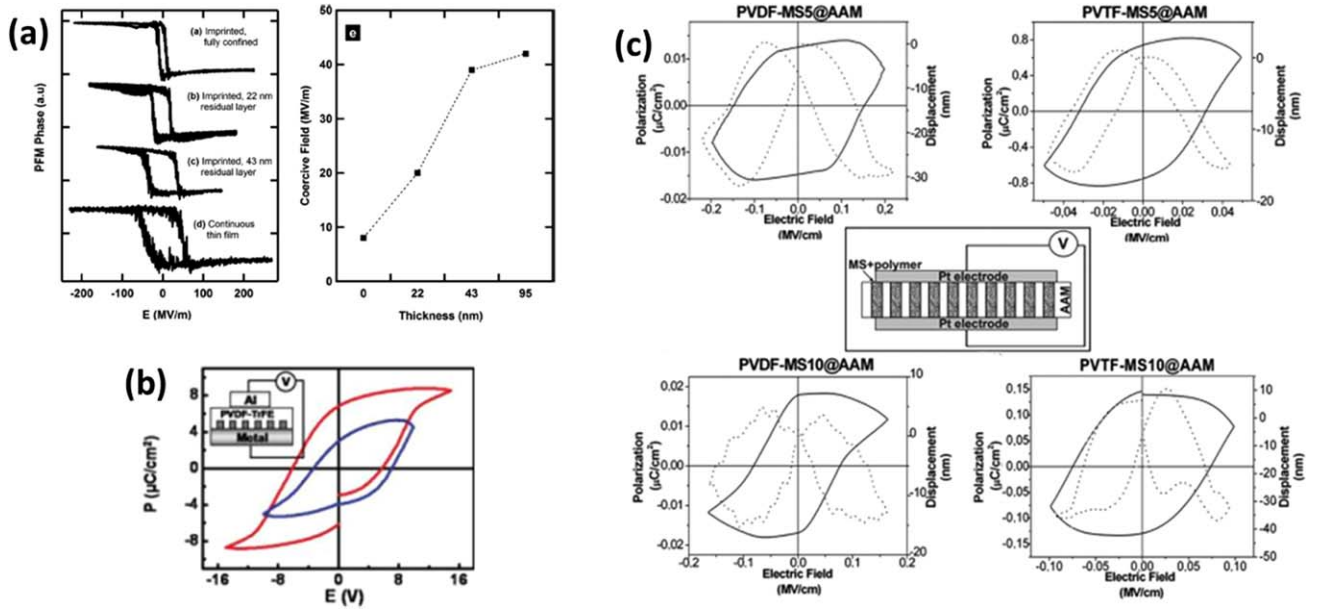

Figure 5. (a) (Left panel) PFM phase piezoresponse hysteresis loops of arrays of nanopillars with different residual layer thicknesses and (right panel) the coercive field of the different nanoimprinted samples as a function of the thickness of the residual layer. Reprinted with permission from ref. 54. Copyright 2013 American Chemical Society. (b) Saturated and semisaturated ferroelectric polarization loops of the nanopatterned P(VDF–TrFE) film on the OSte lamellas. Reprinted with permission from ref. 11. Copyright 2013 American Chemical Society. (c) Polarization loops (filled lines) and displacement butterflies (dotted lines) obtained from ultrathin piezoelectric nanowire samples of PVDF (left panels) and P(VDF–TrFE) (right panels) with diameters of 5 nm (top) and 10 nm (bottom) The samples acronyms refer to: PVDF or PVTF (meaning P(VDF-TrFE)) for the polymer type; MS5 or MS10 as the Mesoporous Silica host having pores of either 5 or 10 nm; AAM as Anodic Alumina Membrane, in which the MS and the PVDF or PVTF nanowires are supported. Reprinted with permission from ref. 19. Copyright 2012 American Chemical Society. [Color figure can be viewed in the online issue, which is available at wileyonlinelibrary.com.]

two all-trans chains packed with their dipoles pointing in the same direction (TTTT conformation) and, thus, with the hydrogen and fluorine atoms disposed at the opposite side of the carbon chain.[33,42] In contrast, the copolymer can crystallize only into the β phase, always presenting ferroelectric behavior, because the trifluoroethylene monomer only shows the TTTT conformation.[43,44] In both polymers, ferroelectric switching, induced by a polarity change of an applied electric field, occurs by the facile rotation of the permanent dipole between hydrogen and fluorine atoms disposed on the *b* axis perpendicular to the polymer chain backbone (which is the *c* axis).[7,19] Moreover, for the crystal symmetry considerations made previously, both PVDF and P(VDF–TrFE) also show piezoelectric and pyroelectric properties, a required constraint for being a ferroelectric material. With respect to the most used piezoelectric ceramics, such as PZT and $BaTiO_3$, PVDF and P(VDF–TrFE) have a negative piezoelectric coefficients; this would cause a contraction of the polymeric sample when it is subjected to a positive electric field and vice versa.

Two main methods are commonly used for the characterization of the ferroelectric and piezoelectric properties of these polymers. Piezoresponse force microscopy is a scanning probe technique used for the evaluation of ferroelectric domains down to the nanoscale through the application of an alternate voltage to the samples through a conductive AFM tip and the measurement of the induced vibration.[45–48] In addition to the topographic information, the orientation of the ferroelectric dipole can be extracted from the PFM phase signal, whereas the magnitude of d_{33} is proportional to the PFM amplitude. For the characterization of the macroscopic ferroelectric and piezoelectric properties, the measurement setup is normally composed by a Sawyer–Tower circuit for ferroelectric evaluation, coupled with a laser vibrometer for evaluating the crystal deformation.[49–52]

The ferroelectric properties of the two polymers are the key points for their application in data storage.[9,53–57] Normally, a ferroelectric layer is integrated as a gate in a ferroelectric field-effect transistor (FeFET) to tune the semiconductive channel conduction through the switching of the permanent polarization of the polymeric material.[58,59] The main technological issues limiting the performance of data units based on PVDF and its copolymer are related to the high gate voltage needed for the polarization switching (>15 V). The coercive field of these polymers (~50 MV/m) is indeed much higher with respect to their inorganic oxide counterparts (i.e., PZT, $BaTiO_3$).[60] Moreover, a decrease in the thickness down to the nanoscale would result in a further increase in the coercive field (even up to 125 MV/m)[61] because of the reduction of the crystal size and the increase in the structural defects, including the grain boundaries of semicrystalline polymers, pinholes, and residual solvent trapped in the film.[62] A successful way to solve this problem was investigated in recent years by the nanoconfinement of the ferroelectric polymer in structures with dimensions below the intrinsic size of the crystalline aggregates of the bulk material.[1,7,8,36,63,64] As shown previously, nanoconfinement

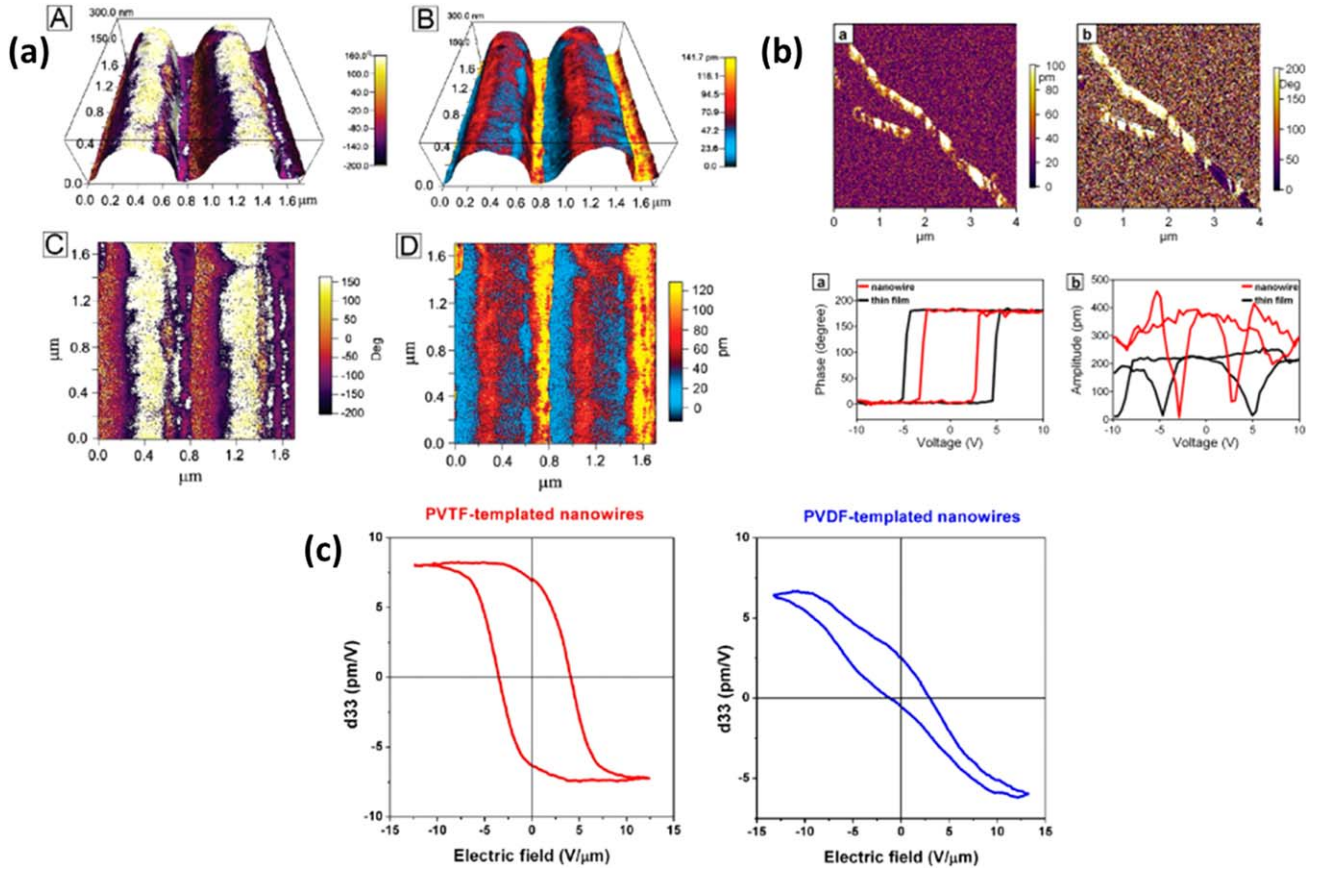

Figure 6. (a) (Top) PFM phase (left panel) and amplitude (right panel) images of the nanoimprinted P(VDF–TrFE) nanopatterned lines imposed on the top of the three-dimensional topography image and (bottom) the corresponding 2D PFM phase and amplitude images. Reprinted with permission from ref. 8. Copyright 2009 American Chemical Society. (b) (Top) PFM amplitude (left panel) and phase (right panel) images of P(VDF–TrFE) synthesized with a template-assisted approach and (bottom) PFM phase and amplitude loops as a function of the tip voltage of a nanowire 60 nm in diameter and a uniform thin film. Reprinted with permission from ref. 33. Copyright 2013 American Chemical Society. (c) d_{33} loops versus the electric field of P(VDF–TrFE) (left panel) and PVDF (right panel) templated nanowires in 200-nm pores of anodic alumina. Reprinted with permission from ref. 18. Copyright 2013 American Chemical Society. [Color figure can be viewed in the online issue, which is available at wileyonlinelibrary.com.]

induces the arrangements of the material in a preferable orientation by the grapho-epitaxial alignment of supramolecular assemblies or by the molecular alignment of confined chains.[7,36] The orientation of the *c* axis of the PVDF polymers, the axis around which the electric dipole rotates, parallel to the substrate facilitates the switching of the polarization upon the application of a vertical electric field. The ease in the switching operation thus leads to an abrupt reduction of the coercive field in the polymeric structure (even two orders of magnitude lower in ultrathin polymeric nanowires[19]). Interestingly, the nanoconfinement not only reduces the formation of structural defects that ease the dipole switching, but it also strongly decreases the leakage current (fundamental in transistor applications) and improves the remnant polarization value close to the bulk value.[1] The configuration used by Hu *et al.*[7] leads to nanoconfined structures with a nanoimprinting technique, as described previously in detail, and facilitates the switching of the electric dipole by an optimal coupling with the electric field; this reduces the coercive field up to 10 MV/m. The improvement of the crystal quality was also confirmed by a comparison of the piezoresponses of the nanocell on unpoled and poled samples. The two measured amplitudes did not change; this indicated an optimum chain organization induced by the nanoconfinement technique. This strong decrease in the coercive field could be experienced only on a fully confined sample, without any residual layer left from the nanoimprinting step. Actually, it was demonstrated that the presence of a residual layer, which normally shows a random domain orientation, would screen the benefits from the nanoconfinement until a coercive field value was reached that was comparable with the uniform film one for a residual film thickness close to half pillar height [as shown in Figure 5(a)].[54]

Exploiting a self-assembled patterning technique, Kang *et al.*[1] reduced the confined structure up to 30 nm by spin coating the P(VDF–TrFE) on an array of OS lamellas. They were able with this structure to fabricate an FeFET for nonvolatile memory application with a strong reduction in the gate leakage voltage and a low programming voltage because of the ease in domain switching [Figure 5(b)].

Table I. Ferroelectric and Piezoelectric Properties of the Nanostructured PVDF and P(VDF–TrFE) Polymer Samples Reported in the Literature

Reference	Technique	Nanostructure	Material	PFM or S-T circuit[a]	Coercive field (MV/m)	Remnant polarization ($\mu C/cm^2$)	$\lvert d_{33}\rvert$ (pm/V)
Cauda *et al.*[19]	Templated-assisted	Ultrathin nanowires	Both	Both	7–15	0.01–0.7	8–22
Cauda *et al.*[18]	Templated-assisted	Nanowires	Both	S-T	5–10	9.6	6.5–8
Kang *et al.*[1]	Templated-assisted	Lamellas	P(VDF-TrFe)	S-T	58	6.8	—
Wu *et al.*[33]	Templated-assisted	Nanowires	P(VDF-TrFe)	PFM	40	—	25–45
Li *et al.*[65]	Templated-assisted	Nanotubes	P(VDF-TrFe)	S-T	164	6.63	—
Wang *et al.*[66]	Templated-assisted	Nanotubes	P(VDF-TrFe)	S-T	16.9	5.7	—
Hu *et al.*[7]	Nanoimprinting	Nanocells	P(VDF-TrFe)	PFM	10	—	—
Park *et al.*[11]	Nanoimprinting	Exagonal pattern	P(VDF-TrFe)	S-T	10 V[b]	5.1	—
Hong *et al.*[6]	Nanoimprinting	Nanograss	P(VDF-TrFe)	PFM	—	—	72.7 (210)[c]
Liu *et al.*[8]	Nanoimprinting	Nanolines and nanocells	P(VDF-TrFe)	PFM	~40	—	48–81
Fang *et al.*[35]	Nanoimprinting	Nanolines	P(VDF-TrFe)	S-T	~70	~13	—
Chen *et al.*[63]	Nanoimprinting	Nanodots	P(VDF-TrFe)	PFM	65	—	X[d]
Kassa *et al.*[64]	Nanoimprinting	Nanocells	P(VDF-TrFe)	PFM	8[e]	—	—
Ong[68]	Nanoimprinting and direct patterning	Nanolines	PVDF	PFM	—	—	16.02

[a] Piezoelectric force microscope or Sawyer–Tower circuit.
[b] Thickness not specified.
[c] Average value (maximum value).
[d] PFM amplitude maps are reported without the d_{33} estimation.
[e] Minimum value obtained on fully confined nanocells.

Similar results have been obtained by the confinement of the two polymers in the nanometric channels of an anodic alumina membrane by several groups.[18,19,33,65,66] In particular, Cauda *et al.*[18] synthesized P(VDF–TrFE) wires in pores with a diameter of 200 nm of an alumina membrane; this resulted in a higher level of crystallization and strongly reduced the coercive electric field necessary to switch the domains. Interestingly, the PVDF nanowires prepared with this approach directly crystallized in the β phase and, thus, presented the piezoelectric phase without a poling step at high temperatures and voltages being performed. This crystallographic orientation was clear evidence of the benefits of nanoconfinement in piezoelectric polymers. The favorable ferroelectric and piezoelectric properties were obtained because of the induced preferred orientation of the chain *c* axis perpendicular to the direction of the pores. The dipole moment of both polymers turned around the *c* axis upon the application of a vertical electric field perpendicular to the channels; thus, the polarization along the long axis of the nanowires was maximized because of the vertical orientation of the polar *b* axis [Figure 1(b)]. Thanks to this configuration, the poling of both the PVDF and P(VDF-TrFE) nanowires was not required to obtain a remarkable piezoelectric response; thus, the high-temperature step, normally carried out upon immersion in silicone oil, which could contaminate the samples, was avoided. The remnant polarization value obtained for these samples was around 8 $\mu C/cm^2$, close to the 7–15 $\mu C/cm^2$ value of the bulk material obtained after a poling step.[56,67] This is a very promising result when one takes into account the fact that only half of the electrode area is composed by piezoelectric material and the other part is constituted by dielectric alumina. A step forward in this nanoconfinement approach was reached by the preparation of ultrathin polymeric nanowires of both PVDF and P(VDF–TrFE), both 5 and 10 nm in diameter and 60 μm in length (hosting membrane thickness).[19] This extreme spatial confinement induced a preferential orientation of the crystalline domains of the polymer into the ferroelectric phase and led to a strong decrease in the coercive electric field as well in this case without the need for an additional poling step [Figure 5(c)]. However, the values of remnant polarization were strongly reduced (up to 0.01–0.7 $\mu C/cm^2$) with respect to the bulk ones because of defects in the mesoporous and alumina membranes, which increased the leakage currents. In addition, only a small percentage of the investigated area comprised the ferroelectric wires, whereas most of the remaining electrode surface consisted of nonpolar oxides.

Even if most of the works in the literature have been focused on the analysis of the ferroelectricity in the nanoconfined PVDF system, the piezoelectric properties are also strongly enhanced by the exploitation of these nanostructurations. It was observed in nanopatterned P(VDF–TrFE) structures [Figure 6(a)] that the

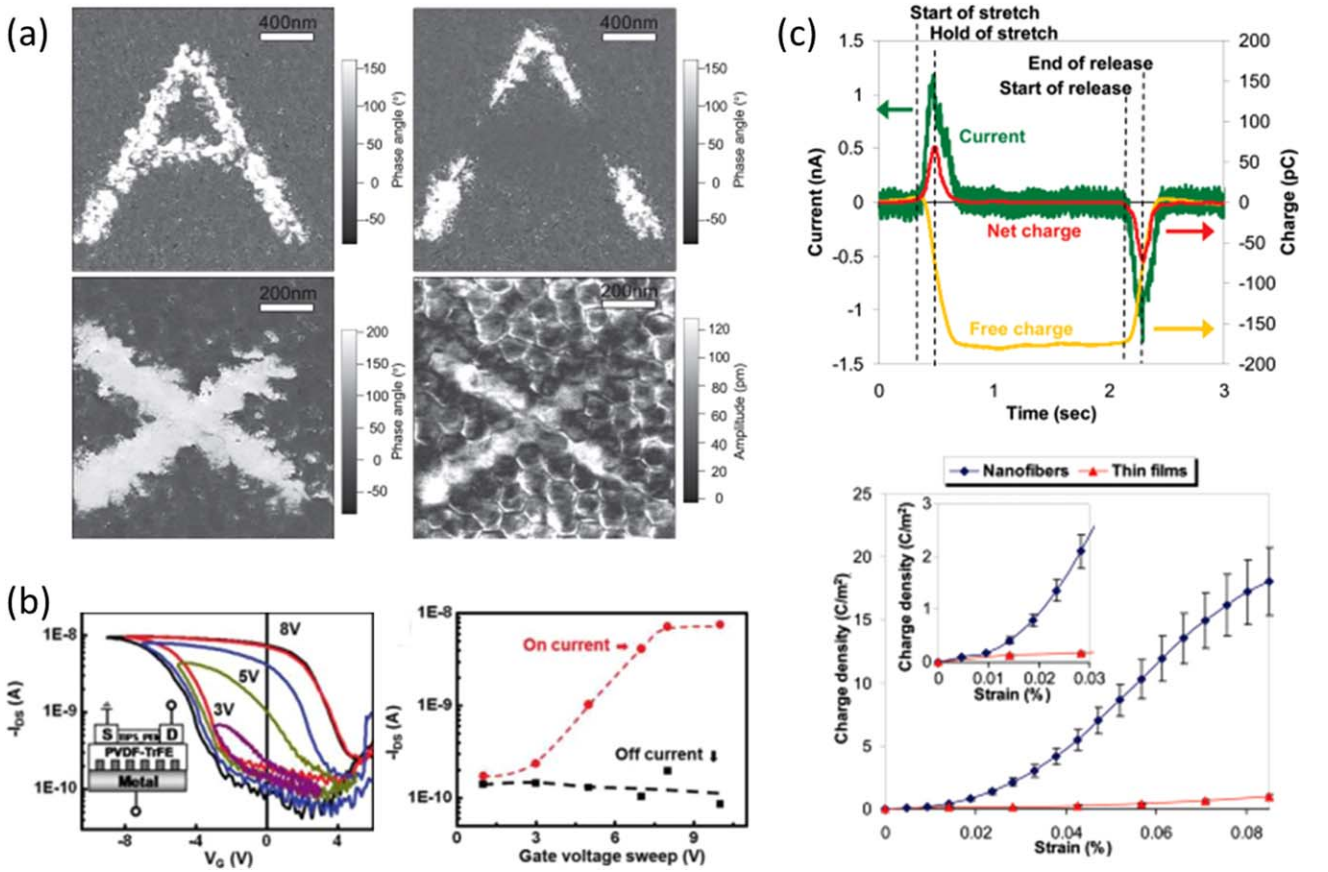

Figure 7. (a) (Top) PFM phase images showing the writing and erasing of an A by the application of an electric field to the nanodot array and (bottom) PFM phase and amplitude images showing an X written on the nanodot arrays by the application of a positive electric field. Reprinted with permission from ref. 63. Copyright 2013 Wiley-VCH. (b) (Left) I_D–V_G (drain current versus gate voltage) curve of the FeFET fabricated with the P(VDF–TrFE) lamellae nanopatterned gate (in the scheme S and D are source and drain electrodes respectively) and (right) on-and-off I_D current as a function of the gate voltage. Reprinted with permission from ref. 1. Copyright 2011 American Chemical Society. (c) (Top) Charge movements during the stretching and release of the PVDF fiber nanogenerator fabricated through electrospinning technique. The green line represents the output current, the yellow line shows the external free charges (electrons) transported from the external wires to the nanogenerator, and the red line shows the measured net charges (holes) of the nanogenerator. Reprinted with permission from ref. 5. Copyright 2010 American Chemical Society. [Color figure can be viewed in the online issue, which is available at wileyonlinelibrary.com.]

nanoimprinting process led to a piezoelectric coefficient in the range of about 41–81 pm/V without any annealing or poling step, as required for uniform thin films.[8] Both the confined dimension and pressure applied during the nanoimprinting process helped the crystallization and the favorable orientation of the polymers. Similarly, in piezoelectric nanowires prepared by the template-assisted approach, an enhancement of the piezoelectric properties with respect to the bulk samples was observed. PFM measurements on individual nanowires with diameters of around 60 nm evidenced d_{33} values in the range 25–45 pm/V without any poling [Figure 6(b)]; this value was larger than in both thin films of the same thickness and bulk samples.[33] In contrast, as shown by a macroscopic characterization, 200-nm [Figure 6(c)] and ultrathin (5–10 nm) nanowires in alumina membranes underwent a slight reduction in d_{33} (6.5–22 pm/V).[18,19] Anyway, it should be taken into account that in this configuration, no poling step was performed with the samples; this would have probably resulted in an increase in the piezoelectric performances. Moreover, two further considerations have to be underlined to justify these worsened performances. First, the displacement of the nanowires could have been reduced by the constriction of the hard and rigid alumina walls. Second, the effective piezoelectric area was greatly lower with respect to the whole electrode one because of the presence of the insulating nonpolar alumina (ca. 50% of the whole surface and even less for ultrathin nanowires). Therefore, the measurement of displacement and, thus, of d_{33} was attenuated because it was generated only by the discrete nanowires and not by a uniform surface.

A comprehensive summary of the piezoelectric and ferroelectric properties described previously is reported in Table I, which facilitates comparison among the different nanostructuration approaches.

APPLICATIONS

Nonvolatile Low-Voltage Memories

The need for data storage is continuously increasing and, at present, dynamic random access memories, hard-disk drives,

and flash memories are in use. However, they present several limitations because dynamic random access memory needs refresh cycles and, thus, extra power supply; hard-disk drives are too slow to access and power-consuming; and flash memory has a limited endurance.[68] Ferroelectric memories have, therefore, been presented in the literature as a possible alternative, mainly because inorganic thin films form complex structures on standard silicon and integrated ones on circuits. They show fast switching, low power consumption, and long durability.[69] However, they also show some disadvantages, like brittleness and fragility. They can be easily damaged during the conventional lithographic process, and in particular, they are not fully compatible with emerging flexible organic electronics. For these reasons, ferroelectric PVDF and P(VDF–TrFE) polymers, having a remnant polarization as high as 10 $\mu C/cm^2$, show promising potential as materials for low-voltage and nonvolatile memories with respect to their inorganic counterparts. In addition, the high flexibility, low cost, and easy processability facilitate their integration as micromaterials and nanomaterials in organic electronic devices. As reported previously, the confinement of such polymers down to the nanoscale induces a preferential orientation of the polar *c* axis; this facilitates the polarization switching upon the application of an electric field and greatly reduces the overall coercive field in the polymeric nanostructure. In addition, thanks to this nanoscale confinement, ferroelectric polymer nanostructures can individually switch and store data through the application of a low bias (in the range of a few volts). This is fully compatible with the needs of standard integrated circuits.

High-density P(VDF–TrFE) nanodots were fabricated by the nanoimprinting technique to obtain highly oriented copolymer chains for easy polarization switching of each single nanodot.[63] Writing and erasing in two dimensions was obtained at high speed by a conducting PFM probe working at low voltages; it reached a resolution of less than 10 nm and, thus, a high data storage density [as high as 75 Gb/in.^{2}; Figure 7(a)].

Similarly, high-density nanocells (>33 Gb/in.^{2}) of P(VDF–TrFE) were obtained by a nanoembossing protocol with well-defined switching behavior from cell to cell and a low operation voltage.[7] Each nanocell showed a low coercive field of about 10 MV/m, which was well below the reported values of bulk materials (50 MV/m) and a narrow square-shaped hysteresis curve with low energy losses.

Kang *et al.*[1] demonstrated a novel nonvolatile polymeric FeFET memory based on a single-crystalline tri-isopropylsilylethynyl pentacene channel and a hybrid gate insulator composed of P(VDF–TrFE) nanoscopic trenches of 30 nm in width confined into self-assembled dielectric OSte lamellae. The authors stated that the confined crystallization of P(VDF-TrFE) not only significantly reduced the gate leakage current but also induced an effective crystal orientation, which facilitated ferroelectric polarization switching. These improved performances were due to the elimination of structural defects and the development of an effective P(VDF–TrFE) crystal orientation through the nanoconfinement process. The device showed a characteristic source-drain current hysteresis, which was fully saturated at a programming voltage of 8 V with an on/off current ratio of 102 and a data retention time of approximately 2 h [Figure 7(b)].

Mechanical Pressure Sensors

PVDF and P(VDF–TrFE) polymers have been proposed as pressure sensors in the detection of applied mechanical deformation.[50,70,71]

PVDF[72] and P(VDF–TrFE)[2] nanofiber webs were fabricated by electrospinning and packed between metalized top and bottom electrodes. In particular, Lee *et al.*[72] reported silver-plated PVDF nanofiber webs as pressure sensors for the monitoring of respiration and muscle movement. Combining the piezoelectric sensor with a capacitive one, they were able to monitor static and dynamic pressure changes during walking at 5 km/h. In another study,[73] the authors used the same sensor for detecting electromyography signals from the contraction and release of muscles.

Energy Nanogenerators

Harvested mechanical energy from the environment is an attractive renewable source of power for various applications.[74,75] In the literature, power generators can be found ranging from large-scale harvesters, that convert mechanical energy into electricity starting from natural events, that is, waterfalls, wind, and ocean waves,[76,77] to small-scale energy harvesters, which scavenge energy from small vibrations derived from automotives, buildings, and human movements.[78,79] Recently, piezoelectric nanostructured polymers have been proposed as energy nanogenerators with high energy conversion efficiencies. Their advantages, with respect to ceramic nanogenerators, such as ZnO or $BaTiO_3$, consist of enhanced flexibility and endurance and the feasibility of their fabrication over a large area,; this leads to improved power generation. A prominent example is the work of Chang *et al.*,[5] who deposited PVDF nanofibers by near-field electrospinning on a flexible substrate and, after mechanical stretching and electrical poling, efficiently generated a remarkable piezoelectric potential upon bending deformation. In particular, when the substrate was stretched and released repeatedly, voltages of 5–30 mV and current outputs of 0.5–3 nA were recorded [Figure 7(c)]. Excellent results were also obtained by Mandal *et al.*[2] from P(VDF–TrFE) electrospun fibers, which formed a web on the substrate and showed peaks of about 400 mV when a sinusoidal pressure was imparted on the device.

CONCLUSIONS AND FUTURE DIRECTIONS

Piezoelectric polymers with nanosized features are an emerging class of materials that can specifically and efficiently respond to applications requiring high flexibility, low processing temperatures, low costs, and durability. The concept of nanostructuration represents a powerful approach for the preparation of piezoelectric arrays of polymeric nanostructures because they are simple, have high throughput, and are cost effective.

This review has shown improvements in the piezoelectric and ferroelectric performances upon confinement to the nanoscale level, thanks to the preferential orientation of the polymeric chain achieved under a confined space. The nanostructures can be obtained generally in a single-step procedure with no need for poling, and this opens up promising applications in ready-to-use devices.

In the future, we envision the complete integration of such nanostructured polymers as energy nanogenerators, ciliated

sensors, and nonvolatile low-voltage memories on printed plastic electrodes; this will lead to cheap, all-plastic, high-density flexible devices, which can be further coupled to current polymer electronic devices, such as displays and digital circuits. Alternatively, ferroelectric nanostructures could also be directly integrated in field-effect transistors, as their low-voltage operation is compatible with the requirements of metal oxide semiconductor technology.

More broadly, the tuning at the macromolecular level of the polymer chain or crystal orientation by nanoconfinement holds promise for the nanostructuration of other materials, such as in the sol–gel processing of ferroelectric precursors or phase changes. Similarly, other applications can be envisioned, such as multiferroic systems, microfluidic nano-actuated devices, smart drug-delivery systems, and other types of nanodevices.

REFERENCES

1. Kang, S. J.; Bae, I.; Shin, Y. J.; Park, Y. J.; Huh, J.; Park, S.-M.; Kim, H.-C.; Park, C. *Nano Lett.* **2011**, *11*, 138.
2. Mandal, D.; Yoon, S.; Kim, K. J. *Macromol. Rapid Commun.* **2011**, *32*, 831.
3. Steinhart, M.; Wendorff, J. H.; Greiner, A.; Wehrspohn, R. B.; Nielsch, K.; Schilling, J.; Choi, J.; Gosele, U. *Science* **2002**, *296*, 1997.
4. Oh, S.; Kim, Y.; Choi, Y.-Y.; Kim, D.; Choi, H.; No, K. *Adv. Mater.* **2012**, *24*, 5708.
5. Chang, C.; Tran, V. H.; Wang, J.; Fuh, Y.-K.; Lin, L. *Nano Lett.* **2010**, *10*, 726.
6. Hong, C.-C.; Huang, S.-Y.; Shieh, J.; Chen, S.-H. *Macromolecules* **2012**, *45*, 1580.
7. Hu, Z.; Tian, M.; Nysten, B.; Jonas, A. M. *Nature Mater.* **2009**, *8*, 62.
8. Liu, Y.; Weiss, D. N.; Li, J. *ACS Nano* **2010**, *4*, 83.
9. Naber, R. C. G.; Tanase, C.; Blom, P. W. M.; Gelinck, G. H.; Marsman, A. W.; Touwslager, F. J.; Setayesh, S.; De Leeuw, D. M. *Nat. Mater.* **2005**, *4*, 243.
10. Xu, L.; Cao, J.; Huang, D. IEEE International Conference on Mechatronics and Automation, ICMA 2005, Niagara Falls: Canada, **2005**; p 1992.
11. Park, Y. J.; Kang, S. J.; Shin, Y.; Kim, R. H.; Bae, I.; Park, C. *Curr. Appl. Phys.* **2011**, *11*, e30.
12. Lin, M. F.; Lee, P. S. *J. Mater. Chem. A* **2013**, *1*, 14455.
13. Priya, A. R. S.; Subramania, A.; Jung, Y.-S.; Kim, K.-J. *Langmuir* **2008**, *24*, 9816.
14. Asano, T.; Kubo, T.; Nishikitani, Y. *J. Photochem. Photobiol. A* **2004**, *164*, 111.
15. Lovinger, A. J. *Science* **1983**, *220*, 1115.
16. Dillon, D. R.; Tenneti, K. K.; Li, C. Y.; Ko, F. K.; Sics, I.; Hsiao, B. S. *Polymer* **2006**, *47*, 1678.
17. Lutkenhaus, J. L.; McEnnis, K.; Serghei, A.; Russell, T. P. *Macromolecules* **2010**, *43*, 3844.
18. Cauda, V.; Stassi, S.; Bejtka, K.; Canavese, G. *ACS Appl. Mater. Interface* **2013**, *5*, 6430.
19. Cauda, V.; Torre, B.; Falqui, A.; Canavese, G.; Stassi, S.; Bein, T.; Pizzi, M. *Chem. Mater.* **2012**, *24*, 4215.
20. Ottone, C.; Bejtka, K.; Chiodoni, A.; Farías, V.; Canavese, G.; Roppolo, I.; Stassi, S.; Cauda, V. *New J. Chem.* **2014**, *38*, 2058.
21. Ottone, C.; Laurenti, M.; Bejtka, K.; Sanginario, A.; Cauda, V. *J. Mater. Sci. Nanotechnol.* **2014**, *1*, s107.
22. Steinhart, M.; Wendorff, J. H.; Wehrspohn, R. B. *Chem. Phys. Chem.* **2003**, *4*, 1171.
23. Cauda, V.; Onida, B.; Platschek, B.; Muhlstein, L.; Bein, T. *J. Mater. Chem.* **2008**, *18*, 5888.
24. Cauda, V.; Mühlstein, L.; Onida, B.; Bein, T. *Micropor. Mesopor. Mater.* **2008**, *118*, 435.
25. Li, Y.; Auras, F.; Löbermann, F.; Döblinger, M.; Schuster, J.; Peter, L.; Trauner, D.; Bein, T. *J. Am. Chem. Soc.* **2013**, *135*, 18513.
26. Camarota, B.; Mann, S.; Onida, B.; Garrone, E. *ChemPhysChem.* **2007**, *8*, 2363.
27. Garcıa-Gutiérrez, M.-C.; Linares, A.; Hernandez, J. J.; Rueda, D. R.; Ezquerra, T. A.; Poza, P.; Davies, R. *J. Nano Lett.* **2010**, *10*, 1472.
28. Ma, Y.; Hu, W.; Hobbs, J.; Reiter, G. *Soft Matter* **2008**, *4*, 540.
29. Sencadas, V.; Gregorio, R.; Lanceros-Méndez, S. *J. Macromol. Sci. Phys.* **2009**, *48*, 514.
30. Qiu, X. *J. Appl. Phys.* **2010**, *108*, 011101.
31. Baskaran, S.; He, X.; Wang, Y.; Fu, J. Y. *J. Appl. Phys.* **2012**, *111*, 014109.
32. Wu, Y.; Li, X.; Weng, Y.; Hu, Z.; Jonas, A. M. *Polymer* **2014**, *55*, 970.
33. Wu, Y.; Gu, Q.; Ding, G.; Tong, F.; Hu, Z.; Jonas, A. M. *ACS Macro Lett.* **2013**, *2*, 535.
34. Park, Y. J.; Kang, S. J.; Park, C.; Kim, K. J.; Lee, H. S.; Lee, M. S.; Chung, U. I.; Park, I. *J. Appl. Phys. Lett.* **2006**, *88*, 242908.
35. Fang, J.-R.; Luo, X.-Y.; Ma, Z.; Shen, Z.-K.; Lu, Q.; Lu, B.-R.; Zhu, G.-D.; Qu, X.-P.; Liu, R.; Chen, Y.-F. *Microelectron. Eng.* **2010**, *87*, 890.
36. Hu, Z.; Baralia, G.; Bayot, V.; Gohy, J.-F.; Jonas, A. M. *Nano Lett.* **2005**, *5*, 1738.
37. Yaman, M.; Khudiyev, T.; Ozgur, E.; Kanik, M.; Aktas, O.; Ozgur, E. O.; Deniz, H.; Korkut, E.; Bayindir, M. *Nat. Mater.* **2011**, *10*, 494.
38. Horiuchi, S.; Tokura, Y. *Nat. Mater.* **2008**, *7*, 357.
39. Lu, F. J.; Hsu, S. L. *Macromolecules* **1986**, *19*, 326.
40. Lee, W. K.; Ha, C. S. *Polymer* **1998**, *39*, 7131.
41. Yoon, K.; Kelarakis, A. *J. Nanomaterials* **2014**, Article ID 367671, 7.
42. Kepler, R. G.; Anderson, R. A. *Adv. Phys.* **1992**, *41*, 1.
43. Furukawa, T. *Phase Transitions* **1989**, *18*, 143.
44. Baltá Calleja, F. J.; González Arche, A.; Ezquerra, T. A.; Santa Cruz, C.; Batallán, F.; Frick, B.; López Cabarcos, E. *Adv. Polym. Sci.* **1993**, *108*, 1.

45. Gruverman, A.; Kolosov, O.; Hatano, J.; Takahashi, K.; Tokumoto, H. *J. Vac. Sci. Technol. B* **1995**, *13*, 1095.
46. Gruverman, A.; Kalinin, S. V. *J. Mater. Sci.* **2006**, *41*, 107.
47. Kalinin, S. V.; Bonnell, D. A. *Phys. Rev. B* **2002**, *65*, 1254081.
48. Kalinin, S. V.; Rar, A.; Jesse, S. *IEEE Trans. Ultrason. Ferroelectr. Freq. Control* **2006**, *53*, 2226.
49. Miller, S. L.; Nasby, R. D.; Schwank, J. R.; Rodgers, M. S.; Dressendorfer, P. V. *J. Appl. Phys.* **1990**, *68*, 6463.
50. Canavese, G.; Stassi, S.; Cauda, V.; Verna, A.; Motto, P.; Chiodoni, A.; Marasso, S.; Demarchi, D. *IEEE Sens. J.* **2013**, *14*, 2237.
51. Bouregba, R.; Vilquin, B.; Le Rhun, Q.; Poullain, G.; Domenges, B. *Rev. Sci. Instrum.* **2003**, *74*, 4429.
52. Pecherskaya, E. A. *Measurement Tech.* **2007**, *50*, 1101.
53. Auciello, O.; Scott, J. F.; Ramesh, R. *Phys. Today* **1998**, *51*, 22.
54. Nougaret, L.; Kassa, H. G.; Cai, R.; Patois, T.; Nysten, B.; Van Breemen, A. J. J. M.; Gelinck, G. H.; De Leeuw, D. M.; Marrani, A.; Hu, Z.; Jonas, A. M. *ACS Nano* **2014**, *8*, 3498.
55. Naber, R. C. G.; Asadi, K.; Blom, P. W. M.; De Leeuw, D. M.; De Boer, B. *Adv. Mater.* **2010**, *22*, 933.
56. Heremans, P.; Gelinck, G. H.; Müller, R.; Baeg, K. J.; Kim, D. Y.; Noh, Y. Y. *Chem. Mater.* **2011**, *23*, 341.
57. Ling, Q. D.; Liaw, D. J.; Zhu, C.; Chan, D. S. H.; Kang, E. T.; Neoh, K. G. *Prog. Polym. Sci. (Oxford)* **2008**, *33*, 917.
58. Zheng, Y.; Ni, G. X.; Toh, C. T.; Tan, C. Y.; Yao, K.; Özyilmaz, B. *Phys. Rev. Lett.* **2010**, *105*, 166602.
59. Kanashima, T.; Katsura, Y.; Okuyama, M. *Jpn. J. Appl. Phys.* **2014**, *53*, 04ED11.
60. Haertling, G. H. *J. Am. Ceram. Soc.* **1999**, *82*, 797.
61. Kimura, K.; Ohigashi, H. *Jpn. J. Appl. Phys.* **1986**, *25*, 383.
62. Naber, R. C. G.; Blom, P. W. M.; Marsman, A. W.; De Leeuw, D. M. *Appl. Phys. Lett.* **2004**, *85*, 2032.
63. Chen, X. Z.; Li, Q.; Chen, X.; Guo, X.; Ge, H. X.; Liu, Y.; Shen, Q. D. *Adv. Funct. Mater.* **2013**, *23*, 3124.
64. Kassa, H. G.; Cai, R.; Marrani, A.; Nysten, B.; Hu, Z.; Jonas, A. M. *Macromolecules* **2013**, *46*, 8569.
65. Li, X.; Lim, Y. F.; Yao, K.; Tay, F. E. H.; Seah, K. H. *Phys. Chem. Chem. Phys.* **2013**, *15*, 515.
66. Wang, C.-C.; Shen, Q.-D.; Tang, S.-C.; Wu, Q.; Bao, H.-M.; Yang, C.-Z.; Jiang, X.-Q. *Macromol. Rapid Commun.* **2008**, *29*, 724.
67. Omote, K.; Ohigashi, H.; Koga, K. *J. Appl. Phys.* **1997**, *81*, 2760.
68. Ong, W.; Ke, C.; Lim, P.; Kumar, A.; Zeng, K.; Ho, G. W. *Polymer* **2013**, *54*, 5330.
69. Scott, J. F. *Science* **2007**, *315*, 954.
70. Donato, M. D.; Bocchini, S.; Canavese, G.; Cauda, V.; Lombardi, M. *Key Eng. Mater.* **2014**, *605*, 263.
71. Chiolerio, A.; Lombardi, M.; Guerriero, A.; Canavese, G.; Stassi, S.; Gazia, R.; Cauda, V.; Manfredi, D.; Chiodoni, A.; Verna, A.; Cocuzza, M.; Montanaro, L.; Pirri, C. F. *J. Mater. Sci.* **2013**, *78*, 6943.
72. Lee, S.; Ahn, Y.; Prabu, A.; Kim, K. *J. Fiber Bioeng. Informatics* **2013**, *6*, 369.
73. Ahn, Y. J.; Yoon, S.; Kim, K. *J. Text. Sci. Eng.* **2012**, *49*, 47.
74. Wang, Z. L.; Song, J. *Science* **2006**, *312*, 242.
75. Rivera, V. F.; Auras, F.; Motto, P.; Stassi, S.; Canavese, G.; Celasco, E.; Bein, T.; Onida, B.; Cauda, V. *Chem. Eur. J.* **2013**, *19*, 14665.
76. Lu, X.; McElroy, M. B.; Kiviluoma, J. *Proc. Natl. Acad. Sci. U.S.A.* **2009**, *106*, 10933.
77. Scruggs, J.; Jacob, P. *Science* **2009**, *323*, 1176.
78. Paradiso, J. A. S. T. *IEEE Pervasive Comput.* **2005**, *4*, 18.
79. Yang, R.; Qin, Y.; Li, C.; Zhu, G.; Wang, Z. L. *Nano Lett.* **2009**, *9*, 1201.
80. Lau, S. T.; Zheng, R. K.; Chan, H. L. W.; Choy, C. L. *Mater. Lett.* **2006**, *60*, 2357.